Talanta 82 (2010) 508–515

Contents lists available at ScienceDirect

Talanta

journal homepage: www.elsevier.com/locate/talanta

Hybrid plasma bonding for void-free strong bonded interface of silicon/glass at 200 °C

M.M.R. Howlader[a,*], M.G. Kibria[a], F. Zhang[a], M.J. Kim[b]

[a] Department of Electrical and Computer Engineering, McMaster University, 1280 Main Street West, Hamilton, ON L8S 4K1, Canada
[b] Department of Materials Science and Engineering, University of Texas at Dallas, Dallas, TX 75080, USA

ARTICLE INFO

Article history:
Received 25 January 2010
Received in revised form 4 May 2010
Accepted 5 May 2010
Available online 11 May 2010

Keywords:
Hybrid plasma bonding
Sequential plasma activation
Anodic bonding
Interfacial voids
Bonding strength
Hydrophilicity
Surface roughness
Electrostatic force
High-resolution transmission electron microscopy

ABSTRACT

A novel hybrid plasma bonding (HPB) that combines sequential plasma activation (reactive ion etching followed by microwave radicals) with anodic bonding has been developed to achieve void-free and strong silicon/glass bonding at low temperature. The interfacial voids were observed at the silicon/glass interface both in the anodic bonding and in the plasma activated anodic bonding, but the voids were completely disappeared in the HPB method at 200 °C. The bonding strength of the silicon/glass in the HPB was as high as 30 MPa at 200 °C, which was higher than that in the individual treatment of anodic and plasma activated bonding methods. The improved characteristic behavior of the interface in the HPB is attributed to the higher hydrophilicity and smooth surfaces of silicon and glass after sequential plasma activation. These highly reactive and clean surfaces enhance the mobility of alkaline cations from the glass surface across the interface toward the bulk of glass in the HPB. This transportation resulted in a ~353 nm thick alkaline depletion layer in the glass and enlarged the amorphous SiO_2 across the interface. The void-free strong bonding is attributed to the clean hydrophilic surfaces and the amorphous SiO_2 layer across the interface.

1. Introduction

Anodic bonding has recently attracted much attention to integrate micro/nano-scale lab-on-a-chip devices for separation, sensing and analysis of chemicals (i.e., hydrocarbons, pesticides) and biological species (i.e., DNA, enzymes) [1–3]. One of the requirements for these devices is to utilize excellent physical and chemical properties of glass and silicon (Si). Glass is the material with high biocompatibility, optical transparency, surface hydrophilicity and dielectric property in a wide range of frequency [4]. On the other hand, Si is the most researched material in electronics, which has high thermal conductivity (130 $W m^{-1} °C^{-1}$) with improved on-chip heat dissipation and high mechanical stability [5]. Combining Si with glass through direct bonding allows creating a Si platform required for the integration of future micro/nano-electronic sensing devices. Major challenges of the Si/glass bonding using the existing bonding techniques are the removal of voids (unbonded areas) and high bonding strength of the interface at low temperature (i.e., 150–200 °C). These challenges pose difficulty to fabricate Si and glass based devices with micro/nanofluidic channels for single cell analysis, and separation of DNA molecules [6].

Currently anodic bonding requires heating the contacted wafers in the temperature range of 300–500 °C under applied voltages of 400–1000 V in order to achieve void-free interface with high bonding strength (i.e., 10–15 MPa) [7]. In addition to the high temperature requirement, other approaches, such as adhesive, laser, induction heating, fusion, glass frit, eutectic and solder bonding require chemicals, and high external force for bonding [8]. The high temperature interferes with immobilized chemicals [9], hinders bonding of nanostructures (i.e., nanofluidic channel with integrated nanotubes) [10] due to wafer bow caused by thermal stress [11] and poses design constraints for devices with aluminum or copper integrated circuits [7]. In order to reduce the bonding temperature with improvement of bonding strength, Si and glass surfaces were treated with plasma followed by anodic bonding. The bonding strength achieved through this process was very low (~3.3 MPa) [12], which needs to be improved for practical applications. Furthermore, surface roughness controls bonding strength as well as nucleates voids at the interface [13]. Rough surface reduces optical transparency of glass (i.e., at extreme ultraviolet wavelength) [14], which is crucial in applications where transmitted and reflected optical signals are used for the analysis of chemical or biological species [3,15]. These issues have not been yet

* Corresponding author.
E-mail address: mrhowlader@ece.mcmaster.ca (M.M.R. Howlader).

0039-9140/$ – see front matter © 2010 Elsevier B.V. All rights reserved.
doi:10.1016/j.talanta.2010.05.001

Table 1
List of bonding experiments and their processing conditions.

Bonding method	Bonding temperature (°C)	Applied voltage (kV)	Cold rolling (CR) (0.2 MPa)/external pressure (EP) (0.07 MPa)
1. Anodic bonding	100	1	EP
	150	1	EP
	200	1	EP
2. O_2 RIE plasma activated bonding	Room temp.	No	CR
3. O_2 RIE plasma activated anodic bonding	200	1	CR followed by EP
4. Sequential plasma activated bonding (SPAB)(O_2 RIE activation + N_2 MW activation)	Room temp.	No	CR
5. Hybrid plasma bonding (HPB) (O_2 RIE activation + N_2 MW activation + anodic bonding)	100	1	CR followed by EP
	150	1	CR followed by EP
	200	1	CR followed by EP

addressed for the realization of the micro/nano-scale lab-on-a-chip devices.

This article reports a void-free Si/glass interface with high bonding strength at 200 °C using a novel hybrid plasma bonding (HPB) method. The HPB consists of three steps: (1) surface activation by oxygen (O_2) reactive ion etching (RIE) plasma followed by (2) surface activation by microwave (MW) nitrogen (N_2) radicals and (3) then contact the activated wafers followed by anodic bonding in air. The bonding method that combines the surface activation mentioned in the first two steps is known as the sequentially plasma activated bonding (SPAB). The performance of the interface in the HPB is compared with that in the anodic bonding, O_2 RIE plasma activated bonding, O_2 RIE plasma activated anodic bonding (RIE plasma activation followed by anodic bonding) and SPAB. To gain insight into the HPB mechanism and performance of Si/glass bonded interface, tensile pulling tester, drop shape analyzer, high-resolution transmission electron microscopy (HRTEM) and atomic force microscopy (AFM) have been utilized.

2. Experimental

2.1. Specimens

Commercially available CZ-grown one-side polished 4-in. 525 ± 25 μm thick, p-type (100) Si wafers and double side polished Pyrex 7740 borosilicate 4-in. 500 ± 25 μm thick glass wafers have been used. P-type Si has been chosen because of its higher rate of formation of intimate contact with glass than that of the n-type Si [16].

2.2. Development of hybrid plasma bonding system

The surface activation and wafer bonding have been accomplished using a wafer level HPB system as shown schematically in Fig. 1. The HPB system accommodates up to 200 mm size wafer. It consists of sequential plasma activation and anodic bonding chambers. The sequential plasma activation chamber consists of bottom and top compartments to generate RIE and MW plasma using O_2 and N_2 gases, respectively. The top and bottom compartments are separated by an ion trapping metallic plate. The metallic plate is grounded. The wafer to be activated is placed on the RF driven electrode. The RIE and MW plasma have been generated at 13.56 MHz and 2.45 GHz, respectively. The RIE plasma is generated by the discharge between the RF electrode and the ion trapping metallic plate. The MW is guided by a metal rectangular waveguide and coupled with a dielectric circular glass (quartz). The MW is thus radiated inside the top compartment resulting in electrical discharges of N_2 gas [17]. The ion trapping metallic plate has holes of diameter 1 mm, which traps charged ions and thus helps producing neutral radicals at the bottom compartment. The O_2 RIE and N_2 MW plasma were chosen because these are most efficient in removing contaminations and producing highly reactive surface, respectively [18,19]. The positive ions in RIE plasma are accelerated by direct current (DC) self-bias voltage and thus remove contaminations, native oxides from the surface by physical sputtering mechanism, whereas the MW neutral radical creates chemically reactive wafer surfaces. The anodic chamber is equipped with high voltage electrodes, and heaters in bonding heads to anodically bond the wafers at temperatures up to 200 °C. The DC applied voltage and time in the anodic bonding are kept constant at 1 kV and 10 min, respectively, regardless of the temperature.

2.3. Plasma activation and bonding

Table 1 shows the list of experiments performed in this study. In case of anodic bonding, as received wafers were contacted in clean room (10,000 class) ambient and then bonded in the anodic bonding chamber at temperatures 100, 150 and 200 °C under an external pressure (EP) of 0.07 MPa using the upper bonding head. In case of O_2 RIE plasma activated bonding, the surfaces were activated using a 50 W O_2 RIE plasma for 15 s at 60 Pa and then bonded in clean room ambient and finally cold-rolled (CR) with 0.2 MPa pressure. In O_2 RIE plasma activated anodic bonding, the surfaces were activated using a 50 W O_2 RIE plasma for 15 s at 60 Pa and bonded in anodic bonding chamber at 200 °C. In the sequential plasma activated bonding (SPAB), the surfaces were activated using a 50 W O_2 RIE plasma for 15 s at 60 Pa followed by activation using a 2500 W MW N_2 radicals for 30 s at 60 Pa and then bonded in clean room ambient and finally CR under 0.2 MPa. With these plasma parameters, the self-bias voltage at the substrate electrode was −35 V. The plasma parameters were chosen based on our experience from

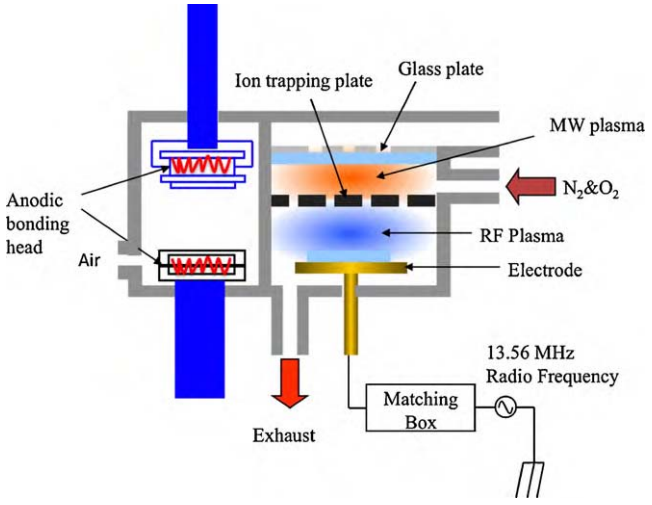

Fig. 1. Hybrid plasma bonding system.

previous study [20]. For HPB, the SPAB specimens went through anodic bonding process at 100, 150 and 200 °C.

2.4. Characterization techniques of bonded interface

For bonding strength measurement, the bonded specimens were diced into 10 mm × 10 mm and glued with copper jigs. The bonding strength measurements were performed for all the bonded specimens shown in Table 1 using a tensile pulling tester from Instron. The hybrid plasma bonded specimen was used for nanointerface observation using an HRTEM. The specimen for HRTEM was prepared using focused ion beam (FIB). For contact angle and surface roughness measurements, two separate sets of specimens were prepared using the plasma parameters as mentioned above. The contact angle of a drop of deionized (DI) water on glass and Si was measured using a drop shape analysis system (DSA100) from Kurss within 5 min after plasma activation. For surface roughness measurement, an atomic force microscope (AFM) from Veeco (ICON) was used. Si tip in tapping mode was utilized over a scanning area of 2 μm × 2 μm.

3. Results and discussion

3.1. Role of temperature in anodic bonding

Fig. 2 shows the optical images of Si/glass specimens anodically bonded at (a) 100, (b) 150 and (c) 200 °C. Voids were present at the interfaces regardless of the bonding temperature. The sizes of the voids were decreased, but their numbers were increased with the increase in the bonding temperature. The anodic bonding currents were zero, 0.01 and 2.9 mA at 100, 150 and 200 °C, respectively, with an applied voltage of 1 kV. At 200 °C, the current was decreased to zero after 10 min. These results indicate that the anodic bonding alone does not provide void-free interface at low temperature. This result is in agreement with the behavior of temperature-dependent voids at the Si/glass interface [21]. In general, the interfacial voids are attributed to (i) hydrogen gas (H_2) from Si oxidation reaction ($Si + H_2O \rightarrow SiO_2 + H_2$) by the adsorbed water (H_2O) on Si and glass wafers or by the water produced at the interface when silanol bonds (Si–OH) are condensed to form siloxane bonds (Si–O–Si), (ii) the entrapment of gas between various bond fronts [7] and (iii) the presence of particles at the interface. The decrease in voids' size and density, as shown in Fig. 2(c), is due to the presence of carbon contaminants, and H_2 caused by temperature enhanced oxidation reaction. The reduction of the voids size with the increase in the temperature is presumably due to the lack of coalescence of voids caused by increase in bonding strength.

3.2. Role of plasma activation on interfacial voids

To achieve void-free interface of Si/glass at low temperature, different combinations between plasma activation and anodic bonding have been systematically investigated. Fig. 3 shows the optical images of the Si/glass wafers bonded using (a) (i) the RIE plasma activated bonding at room temperature and (ii) the RIE plasma activated anodic bonding at 200 °C; (b) (i) the sequentially plasma activated bonding (SPAB) at room temperature and (ii) the sequential plasma activation followed by anodic bonding (HPB) at 200 °C. A comparison of the bonded interfaces in the RIE plasma activated bonding (Fig. 3a(i)), and RIE plasma activated anodic bonding at 200 °C (Fig. 3a(ii)) showed fewer voids at latter interface. After the SPAB (Fig. 3b(i)), the voids were reduced compared to that of the RIE plasma activated bonding. However, void-free interface was achieved at 200 °C in the HPB, as shown in Fig. 3b(ii). Note that the anodic voltage was 1 kV.

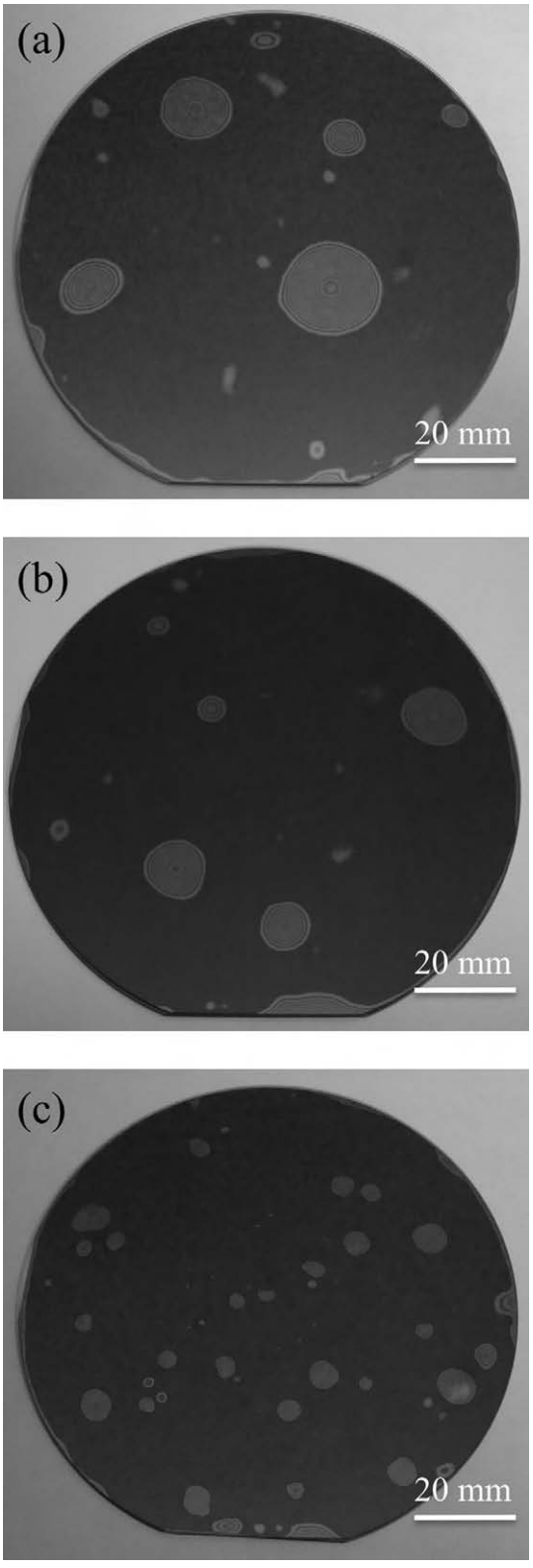

Fig. 2. Optical images of Si/glass wafers anodically bonded at temperature of (a) 100, (b) 150 and (c) 200 °C. Anodic bonding voltage of 1 kV was applied for 10 min.

3.3. Role of plasma activation on bonding strength

Fig. 4 shows a comparative study of bonding strength of Si/glass in the HPB, anodic bonding, RIE plasma activated bonding, RIE plasma activated anodic bonding, and SPAB methods. In the RIE

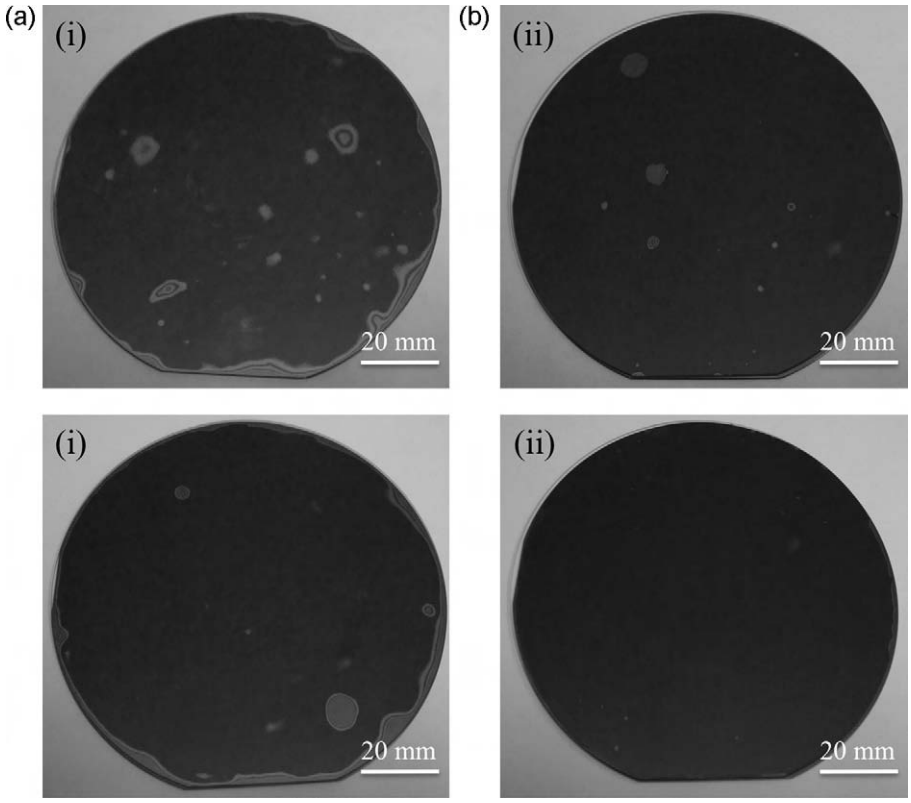

Fig. 3. Optical images of Si/glass wafers bonded through (a) (i) RIE plasma activated bonding and (ii) RIE plasma activated anodic bonding at 200 °C; (b) (i) sequentially plasma activated bonding and (ii) sequential plasma activation followed by anodic bonding (HPB) at 200 °C.

plasma activated bonding and SPAB methods, the specimens were not heated. In the anodic bonding, while the bonding strength was significantly improved from 100 to 150 °C, it was not considerably changed from 150 to 200 °C. The bonding strength of the specimens in the RIE plasma activated anodic bonding at 200 °C was 15 MPa, which was higher than that of the anodic bonding. On the other hand, the bonding strength in the HPB at 100 °C was comparable to that of the anodic bonding at 150 and 200 °C, but lower than that of the RIE plasma activated anodic bonding at 200 °C. With the increase of the bonding temperature in the HPB, the bonding strength was drastically increased. This increase in the bonding strength is in contrast to the increase of the bonding strength in the anodic bonding after plasma activation [12]. At 200 °C, the bonding strength in the HPB was 30 MPa, which was higher compared to that of the anodic, and individual plasma activated bonding and the RIE plasma activated anodic bonding. To the best of the authors' knowledge, the bonding strength was the highest (~30 MPa) number compared to the reported values achieved through the conventional anodic bonding.

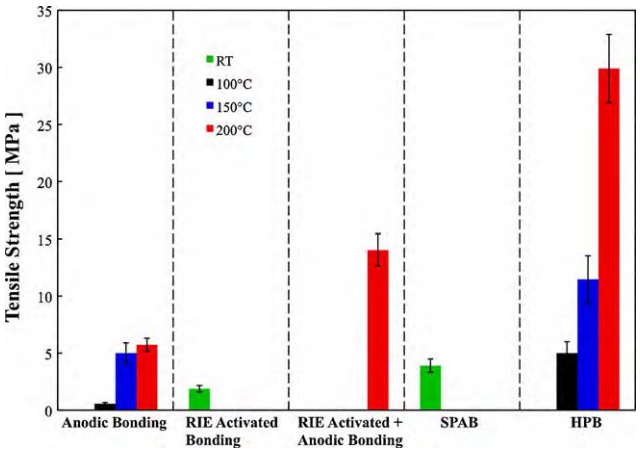

Fig. 4. Bonding strength as a function of different bonding conditions.

Fig. 5 shows the fracture images of Si/glass using (a) the RIE plasma activated anodic bonding and (b) the hybrid plasma bonding at 200 °C. The fracture images show a partial fracture and a complete fracture of glass in the RIE plasma activated anodic bonding and the HPB, respectively, as shown in Fig. 5(a) and (b). It also shows that the fractured glass was remained on Si wafer after the bonding test. On the other hand, in case of anodic bonding, no bulk fracture was observed (not shown). Anodic bonding at all three temperatures (i.e., 100, 150 and 200 °C) resulted in debonding from the interface after tensile pulling test. In case of HPB, bulk fracture of glass occurred at 150 °C (not shown) and 200 °C because of high bonding strength of the interface. This indicates that the bonding temperature has strong impact on the bonding strength. In this study, the impact of the applied voltage on the bonding strength was not investigated. This is because the earlier simulation results showed that the bonding temperature has higher impact over applied voltage on electrostatic force in the anodic bonding. While an increase in applied voltage from 0.2 to 1 kV increased the electrostatic force by 30 times, an increase in bonding temperature from 300 to 400 °C increased the electrostatic force by 6 orders [22]. This implies strong bonding is due to temperature-dependent high electrostatic force. In contrast to the high bond strength in the temperature range of 400–500 °C, we achieved a higher bonding strength (~30 MPa) at a reduced temperature (i.e., 200 °C). The applied voltage was 1 kV. This enhancement of the bonding strength in HPB is caused by the sequential plasma activation. In HPB, the sequential plasma activation removes contaminations and native oxides from the surfaces. The activated

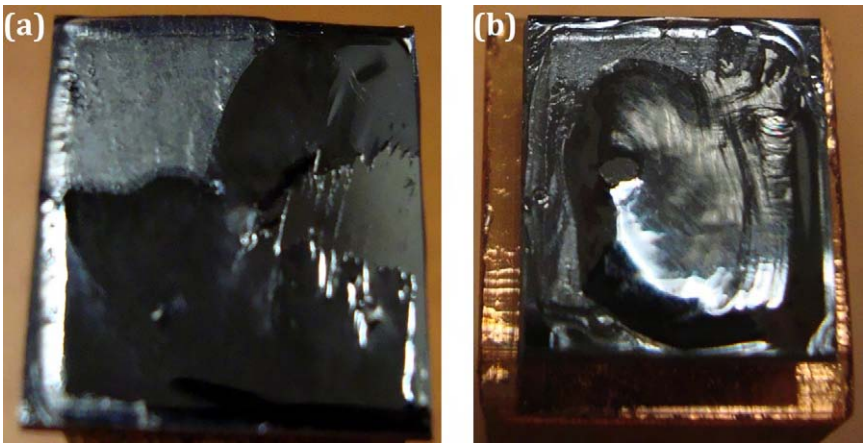

Fig. 5. Fracture images of Si/glass bonded using (a) the RIE plasma activated anodic bonding and (b) the hybrid plasma bonding at 200 °C.

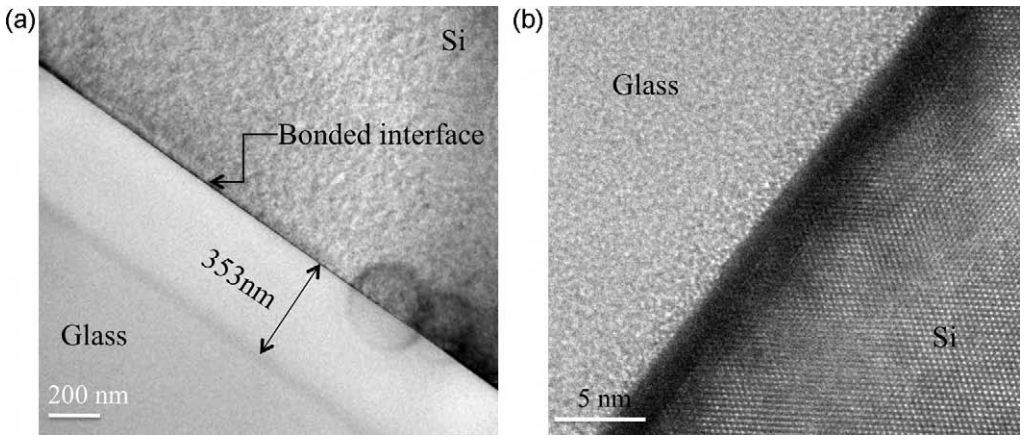

Fig. 6. HRTEM images with (a) low and (b) high magnifications. A ~353 nm thick bright depletion layer in the glass and an indistinct dark edge of Si near the interface are observed.

surfaces in intimate contact result in high electrostatic force under the application of voltage at low temperature in the anodic treatment.

3.4. HRTEM study of hybrid plasma bonded interface

In order to observe the combined effect of plasma activation and electrostatic force, the hybrid plasma bonded Si/glass interface has been investigated using a high-resolution transmission electron microscope (HRTEM). Fig. 6 shows the HRTEM images of hybrid plasma bonded (200 °C) Si/glass interface with (a) low magnification, (b) high magnification. From the low magnification image, a ~353 nm thick layer was identified in glass. This layer was brighter than bulk glass and Si, which was identified as sodium depletion region using energy dispersive X-ray (EDX) spectra [23]. The higher brightness was attributed to the smaller mean atomic number of the depletion region compared to that of the bulk glass, caused by the migration of sodium and potassium cations [7]. The width of this sodium depletion layer in this study was less compared to the most published results [23]. This can be attributed to the low bonding temperature (200 °C) in this study compared to ~350–500 °C used in previous studies. The dark band at the edge of depletion region in glass was due to the accumulation of less mobile potassium cations [7]. From the high magnification image (Fig. 6b), a ~2–3 nm thick indistinct layer was observed. This is because of the charging of the glass wafer during TEM specimen preparation.

3.5. Role of plasma activation on hydrophilicity

To understand the role of plasma activation in the hybrid plasma bonding, the contact angles of water on plasma treated Si and glass surfaces were studied. In general, the lower the contact angle, the higher the hydrophilicity, and the easier the wafer bonding. Higher hydrophilicity refers to higher surface energy and hence higher bonding strength [24]. Fig. 7 shows the contact angle of both Si and glass wafers before and after plasma activation. Contact angles of both Si and glass surfaces significantly decreased after RIE and sequential plasma activation. In fact, RIE plasma removes surface contaminations (particles, carbon, native oxides, etc.) and creates a large number of dangling bonds (free bonds) by physical sputtering process. MW radicals create a highly reactive surface as reported in Ref. [24]. In clean room ambient, this reactive surface is covered with a large number of bonding sites [hydroxyl (OH^-) groups], resulting in a decrease in the contact angle. This implies an increase in surface energy and improvement in bonding strength, which can be observed through the comparison of the bonding strengths in RIE activated bonding and SPAB (Fig. 4). When the reactive surfaces were brought in contact, the OH^- groups of the mating surfaces attracted each other forming a high bonding strength at room temperature.

3.6. Role of plasma activation on surface roughness

As mentioned previously, the surface roughness controls the bonding strength and nucleates voids at the interface [13]. Surface

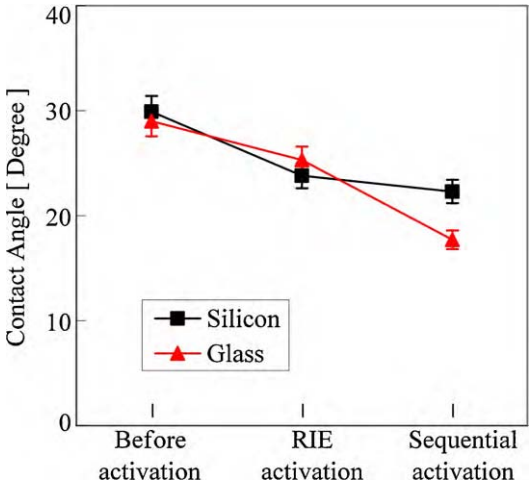

Fig. 7. Contact angle of water on Si and glass before and after plasma activation.

roughness of Si and glass was measured before and after plasma activation to explore the role of plasma activation. Fig. 8 shows the AFM images of surface roughness of Si (a) before plasma activation, (b) after RIE plasma activation, (c) after sequential plasma activation and surface roughness of glass, (d) before plasma activation, (e) after RIE plasma activation and (f) after sequential plasma activation. The root mean square value of surface roughness was measured at 3 locations for each specimen and the average value was estimated. Before plasma activation, the surface roughness of Si was 0.15 nm, which changed to 0.19 nm after RIE plasma activation and to 0.18 nm after sequential plasma activation. On the other hand, the surface roughness of glass was 0.52 nm before activation, 0.48 nm after RIE plasma activation and 0.46 nm after sequential plasma activation. Although the surface roughness of Si was increased after plasma activation, the surface roughness of glass was reduced. This is presumably due to the discrepant etching behavior of Si and glass by the RIE plasma. In contrast to Si, Pyrex glass surface had ~3–5 nm size pits. This surface defects were similar to the plasma induced defects such as nanopores and craters on Si surface which induced void at the Si/Si interface [25]. Therefore, the surface defects were responsible for the void formation as observed by the optical images shown in Fig. 2. The interfacial voids and high surface roughness caused low bonding strength in the anodic bonding, as shown in Fig. 4.

Although there were surface defects on glass, the sequential plasma activation improved (reduced) the surface roughness. This improvement is very important in biosensor applications [3,15], because surface roughness is a measure of surface reflectivity [14]. The lower the surface roughness, the higher the surface reflectivity [14,15]. The reduced surface roughness of glass achieved after sequential plasma activation indicates a higher surface reflectivity. Therefore, the hybrid plasma bonding of Si/glass can be used for the level-free detection of the biological species using optical signal detection [3,15].

4. Hybrid plasma bonding mechanism

In order to explain the hybrid plasma bonding mechanism, it is indispensable to review the current understanding in the anodic bonding [7,21,26,27]. In the anodic bonding, when two polished wafers of Si and glass are brought into intimate contact under DC high voltage (400–1000 V) and high temperature (300–500 °C), the electrostatic force between the materials' surfaces provides permanent chemical bond. The glass and Si are biased by placing on cathode and anode, respectively. The Pyrex glass, being used for anodic bonding, has a coefficient of thermal expansion (CTE) close to Si (i.e., CTE mismatch $<1 \times 10^{-6}\,K^{-1}$) and contains a high concentration of alkali oxides (i.e., Na_2O and K_2O). The glass is negatively charged with respect to the Si. The glass polarizes under these conditions. The alkali oxides dissociate into cations (mainly Na^+) and

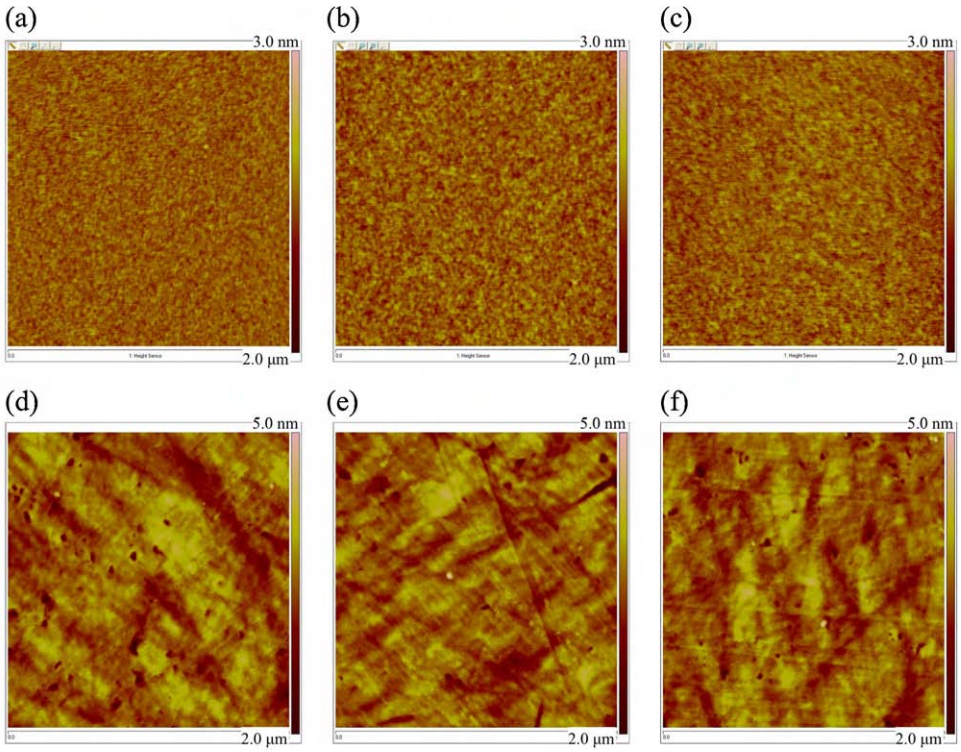

Fig. 8. AFM images of Si (a) before plasma activation, (b) after RIE plasma activation, (c) after sequential plasma activation and of glass, (d) before plasma activation, (e) after RIE plasma activation and (f) after sequential plasma activation.

anions (O^-), then the alkali cations are transported toward cathode resulting in a depletion region in glass, and a thin region of oxygen-rich layer is formed in the vicinity of the interface. Almost the entire applied voltage is shared between the depleted region and the small gap between the two wafers due to surface roughness, and thus the applied voltage generates a high electrostatic force which pulls the mating wafers into intimate contact. Si and glass are thus bonded together due to the high electrostatic force at high voltage and high temperature. The electrostatic force at these conditions is not sufficient to remove the interfacial voids due to the presence of carbon contaminations and native oxides at the interface.

As previously mentioned, the applied voltage has lower impact on the electrostatic force than on the temperature. At 100 °C (Fig. 4), a low electrostatic force resulted in a low bonding strength (0.56 MPa) which allowed the interface gas to move around and coalesce to form larger voids as shown in Fig. 1(a). With increase in temperature, bonding strength improved significantly (5 MPa at 150 °C and 5.73 MPa at 200 °C as in Fig. 4). With increase in temperature, more cations (mainly Na^+) dissociate from Na_2O and K_2O in glass and their mobility increases, resulting in a higher bonding current [18]. The higher current at higher temperature leads to higher electrostatic force and hence improved bonding strength as shown in Fig. 4. The higher bonding strength at higher temperature (i.e., ~200 °C) hindered the movement of entrapped gas at the interface, resulting in smaller void size with increased density, as seen in Fig. 1(c).

On the other hand, void-free interface with high bonding strength was achieved in the HPB. The improvement of the bonding quality in the HPB is due to the surface cleaning, and the augmentation of surface energy of the Si and glass using sequential plasma activation prior to the anodic bonding. In the sequential plasma activation, first, the RIE plasma removes native oxides and surface contaminations, as well as induces an oxide layer (~3–6 nm) on the treated surface [28,29]. Then, the MW nitrogen radicals produce reactive surface with high surface energy [24]. The significant enhancement of the surface energy of glass and Si in the sequential plasma activation was confirmed by using the contact angle measurements. In the HPB, the sequentially plasma activated bonding (SPAB) was performed prior to the anodic bonding. Since the SPAB was done in the air outside the plasma activation chamber, the sequentially treated surfaces were highly hydrophilic due to adsorption of OH^- molecules from the ambient air. This implies that the number of OH^- molecules for bonding remarkably increased after sequential plasma activation [24] resulting in strong adhesion between the surfaces. These OH^- groups form initial contact through hydrogen bonds and finally produce permanent covalent siloxane bonds (Si–O–Si) following the reactions below [24,25].

$$Si–OH + HO–Si \rightarrow Si–O–Si + H_2O \quad (1)$$

$$Si + 2H_2O \rightarrow SiO_2 + 2H_2 \quad (2)$$

When the SPAB specimen went through the anodic bonding, a thick layer of depleted alkaline ions was generated due to the flow of alkali cations toward the cathode, and a thin oxide layer was formed due to reverse flow of oxide anions near the interface. This diffused oxide anions enhance further oxidation of Si under the applied voltage and temperature [30]. The oxidation of Si produces amorphous SiO_2 layer across the interface [27], which absorbs the reaction by-product (H_2) and thus eliminates interfacial voids [29]. In addition, the smooth clean surfaces after the sequential plasma activation were responsible for the void-free interface. Therefore, the void-free high bonding strength in the HPB is due to the combined effect of the adhesion between the large numbers of OH^- groups on the activated surfaces and the electrostatic force produced during the anodic bonding.

5. Conclusions

A novel hybrid plasma bonding system has been developed to achieve void-free Si/glass interface with high bonding strength at 200 °C. Void-free strong bonded interface cannot be realized in the anodic bonding at low temperature due to the presence of surface contaminations and absence of bonding sites (OH^-). Plasma activated bonding itself does not provide void-free strong bonded interface at low temperature due to the absence of electrostatic force. In hybrid plasma bonding (HPB), the electrostatic force in anodic bonding has been combined with high adhesion between the hydrophilic surfaces resulted from the sequential plasma activation to achieve void-free strong bonded interface at low temperature. The improved quality of the bonded interface in the HPB is due to increased bonding sites and smooth surfaces. The highly reactive and clean surfaces enhance the mobility of alkaline cations toward the cathode and the reverse transportation of anions. This transportation resulted in a ~353 nm thick alkaline depletion layer in the glass and enlarged the amorphous SiO_2 across the interface. The void-free strong bonding is attributed to the clean hydrophilic surfaces and the SiO_2 layer across the interface.

Acknowledgements

This research is supported by a discovery grant (No. 327947) from the Natural Science and Engineering Research Council of Canada and an infrastructure grant (No. 12128) from the Canada Foundation for Innovation (CFI). Professor Jamal Deen is greatly appreciated for his support and assistance in establishing nano-bonding and interconnection research at the Micro- and Nano-Systems Laboratory at McMaster University. The authors acknowledge Professor Tadatomo Suga for the development of the sequentially plasma activated bonding method. A. Yamauchi of Bondtech Corporation and G. Kagami of Shinko Seiki Co. Ltd., Japan are acknowledged for their assistance in the construction of the hybrid plasma bonding system.

References

[1] J. Han, H.G. Craighead, Science 288 (2000) 1026.
[2] V. Senez, E. Lennon, S. Ostrovidov, T. Yamamoto, H. Fujita, Y. Sakai, T. Fujii, IEEE Sens. J. 8 (2008) 548.
[3] L.D. Stefano, K. Malecki, A.M. Rossi, L. Rotiroti, F.G.D. Corte, L. Moretti, I. Rendina, Sens. Actuators B 114 (2006) 625.
[4] D.P. Poenar, C. Iliescu, M. Carp, A.J. Pang, K.J. Leck, Sens. Actuators A 139 (2007) 162.
[5] R. Hull, Properties of Crystalline Silicon, INSPEC, London, 1999.
[6] P. Mao, J. Han, Lab Chip 5 (2005) 837.
[7] K.M. Knowles, A.T.J. van Helvoort, Int. Mater. Rev. 51 (2006) 273.
[8] M. Chen, L. Yuan, S. Liu, Sens. Actuators A 133 (2007) 266.
[9] S.C. Jakeway, A.J. de Mello, E.L. Russell, Fresenius J. Anal. Chem. 366 (2000) 525.
[10] K.B. Mogensen, L. Gangloff, P. Boggild, K.B.K. Teo, W.I. Milne, J.P. Kutter, Nanotechnology 20 (2009) 095503.
[11] C.C. Wong, A. Agarwal, N. Balasubramanian, D.L. Kwong, Nanotechnology 18 (2007) 135304.
[12] S.-W. Choi, W.-B. Choi, Y.-H. Lee, B.-K. Ju, M.-Y. Sung, B.-H. Kim, J. Electrochem. Soc. 149 (1) (2002) G8.
[13] M.R. Howlader, Proc. SPIE 7592 (2010) 75920H.
[14] S. Miyagaki, H. Yamanashi, A. Yamaguchi, I. Nishiyama, J. Vac. Sci. Technol. B 22 (2004) 3063.
[15] A. Datta, S. Gangopadhyaya, H. Temkin, Q. Pu, S. Liu, Talanta 68 (2006) 659.
[16] T.M.H. Lee, D.H.Y. Lee, C.Y.N. Liaw, A.I.K. Lao, I.-M. Hsing, Sens. Actuators A (2000) A86.
[17] H. Sugai, I. Ghanashev, M. Nagatsu, Plasma Sources Sci. Technol. 7 (1998) 192.
[18] T Noma, T. Sugiura, K. Ishii, Y. Ohki, Y. Hama, J. Phys. D 30 (1997) 943.
[19] T. Yasuda, Y. Ma, S. Habermehl, G. Lucovsky, J. Vac. Sci. Technol. B 10 (1992) 1844.
[20] M.M.R. Howlader, G. Kagami, T.H. Lee, J.G. Wang, M.J. Kim, A. Yamauchi, J. MEMS, accepted for publication.
[21] J. Wei, S.M.L. Nai, C.K.S. Wong, Z. Sun, L.C. Lee, IEEE Trans. Adv. Pack. 26 (2003) 289.
[22] G.Y. Li, L. Wang, Thin Solid Films 462–463 (2004) 334.
[23] A.T.J. van Helvoort, K.M. Knowles, J.A. Fernie, J. Electrochem. Soc. 150 (10) (2003) G624.

[24] M.G. Kibria, F. Zhang, T.H. Lee, M.J. Kim, M.M.R. Howlader, Nanotechnology 21 (2010) 134011.
[25] M.M.R. Howlader, F. Zhang, M.G. Kibria, J. Micromech. Microeng. 20 (2010) 065012.
[26] Q.F. Xing, M. Yoshida, G. Sasaki, Scripta Mater. 47 (2002) 577.
[27] A.T.J. van Helvoort, K.M. Knowles, R. Holmestad, J.A. Fernie, Philos. Mag. 84 (2004) 505.
[28] M.M.R. Howlader, T. Suga, H. Itoh, T.H. Lee, M.J. Kim, J. Electrochem. Soc. 156 (11) (2009) H846.
[29] X.X. Zhang, J.-P. Raskin, J. Microelectromech. Syst. 14 (2005) 368.
[30] C. Tudryn, S. Schweizer, R. Hopkins, L. Hobbs, A.J. Garratt-Reed, J. Electrochem. Soc. 152 (4) (2005) E131.